Polar Solvation and Solvation Dynamics in Supercritical CHF_3: Results from Experiment and Simulation

Noritsugu Kometani,*,† Sergei Arzhantsev, and Mark Maroncelli*,‡

Department of Applied Chemistry, Graduate School of Engineering, Osaka City University, Sugimoto 3-3-138, Sumiyoshi-ku 558-8585, Japan, and Department of Chemistry, The Pennsylvania State University, University Park, Pennsylvania 16802

Received: November 8, 2005; In Final Form: January 5, 2006

Solvation dynamics of the probe *trans*-4-(dimethylamino)-4′-cyanostilbene (DCS) have been measured in supercritical fluoroform at 310 K (1.04 T_c) and solvent densities over the range $1.4-2.0\rho_c$ using optical Kerr-gated emission spectroscopy. Steady-state measurements and computer simulations of this and the related system coumarin 153 (C153) in fluoroform are used to help interpret the observed dynamics. The solvent contribution to the Stokes shift of DCS is estimated to be 2300 ± 400 cm^{-1} and nearly density independent over the range $(0.7-2.0)\rho_c$. Spectral response functions are bimodal and can be fit to biexponential functions having time constants of ~0.5 ps (85%) and 3−10 ps (15%) over the observable range ($(1.4-2.0)\rho_c$). Computer simulations based on a 2-site model of fluoroform and assuming an electrostatic solvation mechanism appear to properly account for the magnitude and weak density dependence of the Stokes shifts but predict much faster solvation than is observed. Possible reasons for the discrepancy are discussed.

1. Introduction

Solvation in supercritical fluids has been extensively studied from the viewpoint of fundamental physical chemistry as well as in relation to the practical use of supercritical solvents.[1] In both domains, the utility of supercritical fluids results from the fact that modest pressure variations are able to effect large changes in density and thereby relevant solvent properties. Many of the static aspects of solvation in supercritical fluids have now been reasonably well characterized. Most notable is the phenomenon of local density augmentation, the greater than average solvent density surrounding attractive solutes under the highly compressibility conditions pertaining near the solvent's critical point.[2−4] In recent years, more attention has been directed to dynamical aspects of the supercritical fluid environment and how such dynamics influence processes like vibrational dephasing and relaxation,[5−10] translation[11−13] and rotation[14] of solutes, and chemical reactions.[3,15] Central to these latter interests, and the subject of the present report, is "solvation dynamics", the time dependent response of a solvent to perturbations of a dissolved solute. Such dynamics are most often measured by rapidly switching the electronic state of a probe solute using an ultrafast optical pulse and observing how the emission spectrum evolves in time as the solvent surroundings relax to achieve equilibrium with the new solute electronic state. The observable used to quantify the dynamics is the spectral response function

$$S(t) = \frac{\nu(t) - \nu(\infty)}{\nu(0) - \nu(\infty)} = \frac{\Delta E(t) - \Delta E(\infty)}{\Delta E(0) - \Delta E(\infty)} \qquad (1)$$

where $\nu(t)$ is some measure of the frequency of the electronic transition or equivalently the energy gap $\Delta E(t)$ at a time t after the perturbation.

A number of theoretical and simulation studies have recently explored the time dependence of solvation in supercritical fluids.[16−32] Most theoretical treatments have been limited to simplistic models of nonpolar systems such as Lennard-Jones fluids[17,20,22,25] and have adopted a linear response approach, which assumes that the nonequilibrium response embodied in $S(t)$ can be modeled in terms of the fluctuations of the energy gap $\delta\Delta E$ in equilibrium, as described by the correlation function

$$C(t) = \frac{\langle \delta\Delta E(0)\delta\Delta E(t)\rangle}{\langle (\delta\Delta E)^2\rangle} \qquad (2)$$

Simulations of nonpolar systems show that this type of approximation is often reasonably accurate,[19,22] except when large changes to solute−solvent interactions, especially solute size, are involved.[19,23] The response in these nonpolar cases varies with the nature of the solute perturbation,[20,22,26] but typically the dynamics is bimodal, consisting of a fast component related to ballistic and inertial solvent motions and a slower part due to translational diffusion of solvent molecules. For systems involving charged species, for example Xe^+ in Xe,[18,19] or polar solute + solvent combinations,[29,30] large departures from linear response behavior are more frequently encountered. In the case of polar supercritical solvents, both reorientational motions and translational motions of molecules play important roles in the overall response. The comparable importance of both types of dynamics makes the theoretical treatment of polar solvation dynamics especially complex in the case of supercritical fluids. Kapko and Egorov have very recently described a linear response treatment of Stockmayer-like solvent + solute systems that is remarkably accurate.[17] Nevertheless,it is likely that the easiest route to understanding more realistic polyatomic solute and solvent models,[14,33−35] as well as including nonlinear effects, will remain with computer simulation.

In contrast to the considerable body of simulation and theory on solvation dynamics in supercritical fluids, experimental

† Osaka City University.
‡ The Pennsylvania State University.

10.1021/jp0564694 CCC: $33.50
Published on Web 02/14/2006

information on the topic is virtually nonexistent. This situation reflects the difficulty of achieving time resolution adequate to measure these fast dynamics under the conditions of low optical density imposed by low solubilities in supercritical solvents. Apart from an early observation of nanosecond solvation times[36] which probably resulted from solvent impurities, and a study of an AOT microemulsion in near-critical propane,[37] only a single direct measurement of solvation times in supercritical fluids has thus far been published.[38] In that work, Kimura used a streak camera system with a 30 ps response time to measure the dynamic Stokes shift of coumarin 153 in supercritical fluoroform. At 323 K and at densities of 0.4 and 0.8 times the critical density (ρ_c) approximately 10−20% of the relaxation could be detected to occur with a time constant of 60−70 ps. Unpublished work using time-correlated single photon counting (25 ps response time) by our group supports these observations. Also using C153 as a probe in supercritical fluoroform at 308 K, we found that roughly 20% of the expected Stokes shift could be observed at densities between 0.35 and 0.8 ρ_c, with shift times in the range 50−80 ps.[39] In a very recent experiment with ∼20 ps time resolution, Kimura and Saga similarly observed what appears to be a small solvation-induced Stokes shift in a disulfide photoproduct in fluoroform (308 K, 1.2−1.5 ρ_c) having a 50 ps time constant.[40] These experiments, as well as much simulation work, suggest that an experimental method capable of subpicosecond time resolution and also high sensitivity is needed in order to adequately measure solvation dynamics in supercritical fluids.

In present study we use the technique of Kerr-gated emission (KGE) spectroscopy[41] to provide the required combination of time resolution and sensitivity to capture solvation response in supercritical fluoroform. As a solvation probe we chose the solute *trans*-4-(dimethylamino)-4′-cyanostilbene (DCS).[42−45] DCS undergoes a trans−cis isomerization in S_1 on time scales of 100 ps to 2 ns in most solvents.[42,43] Although this isomerization has little effect on the solvation dynamics measured at earlier times,[44,45] the short (∼100 ps) lifetimes it produces in supercritical fluoroform prove highly beneficial for achieving good signal-to-noise with the KGE technique. Herein we describe measurements of DCS in supercritical CHF_3 at a single temperature of 310 K and at densities between 1.4ρ_c and 2.0ρ_c. To provide comparison to the experimental results, we have also undertaken molecular dynamics simulations of DCS as well as C153 in a simplified model of supercritical fluoroform,[46] and these simulation results are also briefly discussed.

2. Experimental Methods

The *trans*-4-(dimethylamino)-4′cyanostilbene (DCS) used in these experiments was obtained from Klaas Zachariasse.[42,43] NMR measurements showed the solid sample of DCS to be better than 95% trans isomer. As described in ref 45, in solution DCS isomerizes upon exposure to UV light, and the samples used here probably contain significantly more than 5% cis isomer. However, we[45] and others[42−44] have not been able to detect emission from *cis*-DCS down to times of less than 100 fs, and thus the presence of the cis form should have little effect on the properties of interest. The CHF_3 used here was purchased from Scott Specialty Gases (99.995%) and was purified by passage through an oxygen trap and a gas dryer prior to use. Steady-state spectroscopic measurements in supercritical CHF_3 were performed using a stainless steel high-pressure cell with three quartz windows and an optical path of approximately 2 cm. After a concentrated solution of DCS was placed in the cell and the solvent removed by evacuation, CHF_3 gas was injected into the cell and maintained at a desired pressure using a syringe pump (ISCO) with a stated accuracy of ±7 kPa. Temperature was controlled by immersing the cell in thermostated water (±0.2 K). The concentration of DCS in supercritical CHF_3 was approximately 2×10^{-6} M. Absorption and corrected emission spectra were recorded using a Hitachi U-3000 UV/vis spectrophotometer and a SPEX Fluorolog F212 fluorimeter, respectively.

A disk-shape stainless steel high-pressure cell with two quartz windows based on the design of Kajimoto and co-workers[47] was constructed for the femtosecond KGE measurements. The optical path length was kept at 2 mm to avoid temporal broadening of instrumental response. DCS and CHF_3 gas were introduced into the cell in the same way as in the steady-state measurements. Temperature was maintained with an accuracy of ±0.2 K using cartridge heaters inserted into the cell body. The sample solution (total volume ∼1 mL) was stirred during measurements using a small magnetic stir bar placed inside the cell. The femtosecond KGE spectrometer has been already described in detail elsewhere.[41] In brief, a mode-lock Ti:sapphire laser (Coherent MIRA-900) combined with a regenerative amplifier (Coherent RegA-9000) was used as the laser source. This system generates 150 fs laser pulses at repetition rate of 250 kHz with energies of about 4 μJ/pulse. The laser pulse was split into two beams. One was frequency doubled by a BBO crystal for sample excitation (387 nm in these experiments) and the other was focused into the Kerr medium (1 mm benzene) located between crossed polarizers to provide the optical Kerr gate. Fluorescence emitting from sample was collected by a parabolic mirror and focused on the Kerr medium with a lens. After passing through the 2nd polarizer, the gated signal was dispersed in a spectrograph + CCD combination. The instrument response of the system, as judged by solvent Raman signals, was 450 fs fwhm.

3. Simulation Methods

Equilibrium molecular dynamics simulations of DCS and C153 in supercritical fluoroform were performed at 310 K and at a series of densities between 0.25ρ_c and 2ρ_c using the DL_POLY program suite.[48] The systems simulated consisted of one solute molecule and 999 or 998 solvent molecules in a cubic periodic box. Simulations were run under constant temperature and pressure conditions using a Hoover-type thermostat and isotropic barostat.[48,49] Short-range interactions were truncated at 12 Å and electrostatic interactions treated with a standard Ewald method.[49] Molecules were modeled as rigid bodies and equations of motion calculated using a Verlet + quaternion algorithm with a step size of 2 fs. Simulations were initiated by inserting the solute into preequilibrated boxes of neat solvent molecules, which were then equilibrated for 2 ns prior to 4 ns of data collection.

All molecular interactions were modeled using sums of site−site Lennard-Jones (12-6) plus Coulomb terms. The solvent model employed was a two-site model of supercritical fluoroform.[46] This model was developed to reproduce the experimental liquid−vapor coexistence curve of fluoroform, and it was also shown to provide good representations of the dielectric constant, viscosity, and other dynamical properties of the real fluid.[46] Solute models were derived from a combination of electronic structure calculations and standard force field parameters. Geometries, assumed to be the same in S_0 and S_1, were obtained from geometry optimizations at the RHF/6-31G(d) level.[50] In the case of C153 the lowest energy, "W-syn" conformation[51] was chosen for optimization. For DCS, the stilbene framework

was constrained to planarity rather than the twisted geometry produced by this level of theory.[45] Ground-state charges were derived from electrostatic potential fits of RHF/6-31G(d) (C153) and MP2/6-311G(d,p) (DCS) wave functions, and charge differences were obtained from semiempirical AM1/CI calculations.[52] These charge differences were used both for calculating the electrostatic part of the spectral shifts as described below and for determining the S_1 charges for running excited-state trajectories. The S_1 charges were calculated as the ab initio charges for S_0 plus these differences. Lennard-Jones parameters for the solute atoms were obtained from the OPLS parameter set.[53] Lennard-Jones parameters for unlike atom interactions were obtained from like atom parameters using the Lorentz−Berthelot combining rules. All potential parameters are provided in Tables S1−S3 of the Supporting Information.

The $S_0 \leftrightarrow S_1$ transitions of DCS and C153 are accompanied by large changes in dipole moment (~13 D in DCS[45,54] and 7 D in C153[55,56]), and for this reason their solvatochromism and dynamic Stokes shifts are primarily determined by the solvent response to these (permanent) dipole moment changes. To model the spectroscopy, we work within the linear response approximation and consider equilibrium fluctuations in the electrical energy differences:

$$\Delta E_{\mathrm{el}} = \frac{1}{4\pi\epsilon_0}\sum_{i,\alpha}\frac{\Delta q_\alpha q_i}{|\vec{r}_\alpha - \vec{r}_i|} \tag{3}$$

where Δq_α and $\vec{r}_\alpha$ are the S_1-S_0 charge difference and position of solute site α, and q_i and $\vec{r}_i$ are the charge and position of solvent site i. ϵ_0 is the permittivity of free space. The solvent-induced shifts in the absorption and emission frequencies of the chromophores are assumed to be given by

$$h\nu_{\mathrm{abs}} - h\nu_{\mathrm{abs}}^{\mathrm{gas}} = \langle \Delta E_{\mathrm{el}} \rangle_0 \tag{4}$$

$$h\nu_{\mathrm{em}} - h\nu_{\mathrm{em}}^{\mathrm{gas}} = \langle \Delta E_{\mathrm{el}} \rangle_1 \tag{5}$$

where the subscripts "0" and "1" denote averaging over trajectories in equilibrium with the S_0 and S_1 solute charge distributions, respectively. The magnitude of the solvent contribution to the Stokes shift $\Delta\nu$ is calculated via

$$\begin{aligned}\Delta\nu &= (h\nu_{\mathrm{abs}} - h\nu_{\mathrm{em}}) - (h\nu_{\mathrm{abs}}^{\mathrm{gas}} - h\nu_{\mathrm{em}}^{\mathrm{gas}}) \\ &= \langle \Delta E_{\mathrm{el}} \rangle_0 - \langle \Delta E_{\mathrm{el}} \rangle_1 \\ &\cong \frac{\langle \delta\Delta E_{\mathrm{el}}{}^2 \rangle_0}{k_{\mathrm{B}}T} \cong \frac{\langle \delta\Delta E_{\mathrm{el}}{}^2 \rangle_1}{k_{\mathrm{B}}T}\end{aligned} \tag{6}$$

The last line of eq 6 is the linear response relationship between the net energy shift induced by the Δq perturbation and the fluctuation of the energy gap, $\delta\Delta E_{\mathrm{el}} = \Delta E_{\mathrm{el}} - \langle \Delta E_{\mathrm{el}} \rangle$, monitored in either solute state. The time dependence of the solvation response, as reported by the spectral response function $S_\nu(t)$ (eq 1) is estimated from the equilibrium time correlation function

$$C_{\Delta E}^{(0,1)}(t) = \frac{\langle \delta E_{\mathrm{el}}(t)\delta E_{\mathrm{el}}(0) \rangle_{0,1}}{\langle \delta\Delta E_{\mathrm{el}}^2 \rangle_{0,1}} \tag{7}$$

The subscripts "0,1" here indicate that, as in the case of $\Delta\nu$, the dynamics can be estimated from the time-dependent fluctuations observed in either the S_0 or the S_1 states.

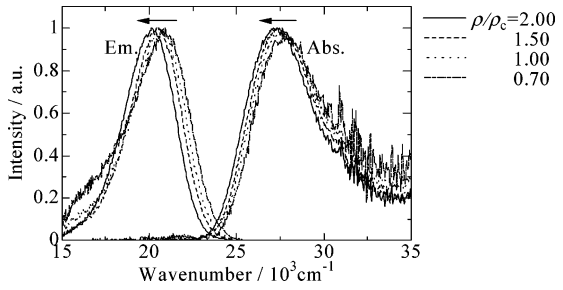

Figure 1. Absorption and emission spectra of DCS in supercritical CHF_3 at 310 K and the densities indicated. Arrows show the direction of increasing solvent density. Excitation wavelength is 25.8×10^3 cm^{-1} (387 nm).

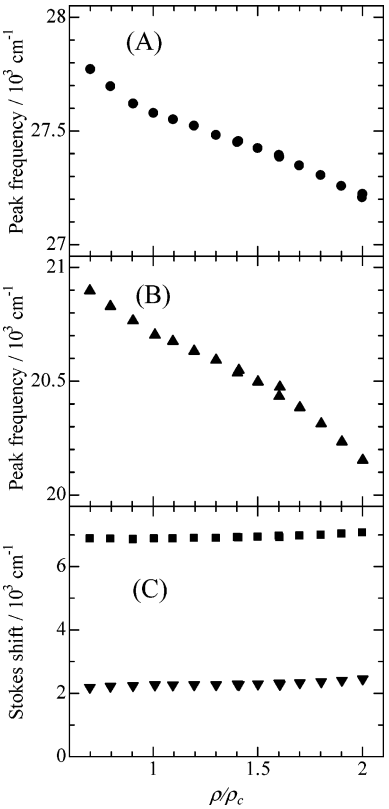

Figure 2. Peak frequencies of (A) the absorption band, ν_{abs}, and (B) the emission band, ν_{em}, of DCS in supercritical CHF_3 at 310 K as a function of density. (C) Stokes shift calculated by $\Delta\nu = \nu_{\mathrm{abs}} - \nu_{\mathrm{em}}$ (filled squares) and $\Delta\nu_s = \nu(\infty)_{\mathrm{est}} - \nu_{\mathrm{em}}$ (downward triangles) as functions of density.

4. Experimental Results and Data Analysis

Figure 1 shows absorption and emission spectra of DCS in supercritical CHF_3 at 310 K and several densities. A single band appears at about 27 000 cm^{-1} in absorption and at 20 100 cm^{-1} in emission. (The shoulder developing near 17 000 cm^{-1} on the emission band is due to an unidentified impurity only evident when the solubility of DCS is very low.) Both the absorption and emission bands shift to lower frequencies with increasing density. The peak frequencies, ν_{abs} and ν_{em}, are plotted as functions of density in Figure 2. The behavior of ν_{abs} and ν_{em} are similar to one another and show the characteristic sigmoidal density dependence indicative of local density augmentation in the near-critical regime. The Stokes shifts, $\Delta\nu = \nu_{\mathrm{abs}} - \nu_{\mathrm{em}}$, are plotted as a function of density in Figure 2C. $\Delta\nu$ is nearly constant over the range $\rho = (0.7-1.2)\rho_c$ and slightly increases with density for $\rho > 1.3\rho_c$. To separate the total Stokes shift into solvation and intramolecular vibrational contributions, we

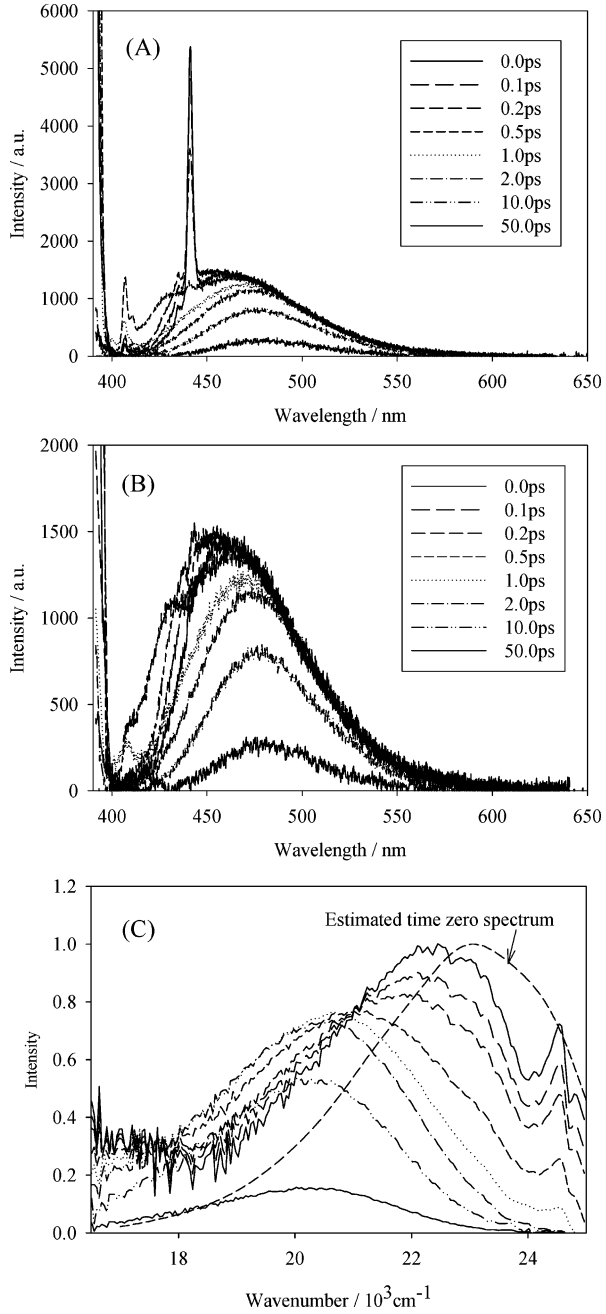

Figure 3. Kerr-gate spectra of DCS in supercritical CHF_3 at 310 K, $\rho/\rho_c = 1.6$ and the indicated delay times: (A) spectra from raw data; (B) spectra after subtraction of solvent Raman bands; (C) spectra after deconvolution analysis and spectral correction.

estimated the time-zero emission spectra prior to any solvent relaxation based on steady-state spectra.[57] The solvent contribution to the Stokes shift is then calculated by $\Delta\nu_s = \nu(0)_{est} - \nu_{em}$, where $\nu(0)_{est}$ denotes the peak frequency of the estimated time-zero spectrum. These values of $\Delta\nu_s$ are also plotted in Figure 2C. The values of $\Delta\nu_s$ are about one-third of the total Stokes shifts, 2300 ± 400 cm^{-1}, and they also vary little with solvent density. This insensitivity of the Stokes shift or equivalently of the reorganization energy associated with the $S_0 \leftrightarrow S_1$ transition to density is at first glance surprising. However, such behavior has also been observed in several other systems[38,58−60] where it is found to extend to even lower densities than are accessible with DCS.

Figure 3 shows typical KGE spectra of DCS in supercritical CHF_3 (T =310K and $\rho/\rho_c = 1.6$). Figure 3A displays the raw spectra obtained from the KGE experiment. In addition to the emission band of DCS observed between 430 and 550 nm, these spectra also exhibit sharp solvent Raman peaks at 410 and 445 nm at early times. These raw spectra were analyzed in the following manner. First the Raman bands were removed by subtracting KGE spectra of pure supercritical CHF_3 from those of the DCS solutions. The results are shown in Figure 3B. To deconvolute the temporal broadening of the spectra due to the instrumental response, as well as to correct the temporal dispersion due to the wavelength-dependent refractive index of the optics and sample, we next fitted the decay curves at all wavelengths to the following convolution function

$$I(t,\lambda) = \int_{-\infty}^{t} dt'\, R(t - t_0(\lambda) - t') \sum_{i=1}^{3} a(\lambda)_i e^{-t'/\tau_i} \qquad (8)$$

where λ denotes wavelength, $R(t)$ is the instrument response function determined by the temporal profile of the Raman band of pure supercritical CHF_3, τ_i is the ith component time constant, and t_0 is the shift of time zero. The fit was first performed on data near 450 nm. The decays at longer wavelengths were then fit to eq 8 by fixing the decay constants τ_i to the values obtained at 450 nm while varying $a_i(\lambda)$ and $t_0(\lambda)$. Finally, time-resolved spectra were reconstructed using the fit parameters and corrected for the spectral sensitivity of the instrument. Figure 3C shows the spectra resulting from this deconvolution analysis. It is evident that the spectral band shifts toward lower frequency with time. There is also a substantial decrease in the intensity of the emission over the 50 ps window displayed here. Time-correlated single photon counting measurements show approximately single exponential decays of DCS emission with time constants of about 100 ps over the density range studied here. The intensity decrease observed in the Kerr experiments was about twice that expected based on this lifetime, apparently as a result of a slight misalignment of the delay line that was not noticed until the experiments were completed.

Also shown in Figure 3C is an estimate of the "time-zero spectrum", the spectrum expected after vibrational relaxation but before any solvent relaxation has occurred. This spectrum is estimated from comparing steady-state spectra in polar and nonpolar solvents[57] and, in the case of DCS, it is expected to provide estimates of the initial frequency needed for constructing $S_\nu(t)$ accurate to roughly ± 300 cm^{-1}. Comparison of such estimated time-zero spectra to the deconvoluted Kerr data indicates that almost all of the solvation dynamics has been captured in these experiments. Given that we excite with $\sim$1000 cm^{-1} excess energy in these experiments, it might be that some more subtle aspects of the spectral changes we observe are related to vibrational cooling of the probe rather than to solvation dynamics. However, on the basis of earlier work in liquid solvents,[61] we do not expect effects related to this cooling to significantly alter the time dependence of the peak frequency of the spectrum, which we attribute solely to solvation dynamics.

To determine emission frequencies, spectra such as those in Figure 3C were fit to a log−normal function. The temporal variation of the peak frequencies $\nu(t)$ are plotted at several densities in Figure 4. These data show $\nu(t)$ to be biphasic, consisting of a major fast component of about 0.5 ps and a minor slow component in the 3−10 ps range. Table 1 summarizes the characteristic parameters obtained by fitting the $\nu(t)$ data with a double-exponential function

$$\nu(t) = [\nu(0) - \nu(\infty)]\{a_1 \exp(-t/\tau_1) + (1 - a_1)\exp(-t/\tau_2)\} + \nu(\infty) \qquad (9)$$

TABLE 1: Parameters Obtained from Fits of $\nu(t)$ of DCS in CHF_3 According to Eq 9[a]

ρ/ρ_c	$\nu(0)/10^3$ cm^{-1}	$\nu(\infty)/10^3$ cm^{-1}	$\nu(0)_{est}/10^3$ cm^{-1}	a_1	τ_1/ps	τ_2/ps	$\langle\tau\rangle$/ps
1.4	22.23	20.33	22.83	0.846	0.63	10.62	2.16
1.4	22.78	20.21	22.81	0.951	0.57	10.02	1.04
1.6	22.60	20.24	22.77	0.859	0.42	3.55	0.86
1.6	22.52	20.22	22.76	0.839	0.47	3.41	0.94
1.8	22.49	20.09	22.68	0.888	0.46	4.89	0.96
2.0	22.05	19.89	22.60	0.928	0.53	7.87	1.06

[a] $\nu(0)_{est}$ is the frequency expected for the spectrum prior to any solvent relaxation based on estimates using the steady-state spectra.[57] $\langle\tau\rangle$ is the integral time $\langle\tau\rangle = a_1\tau_1 + (1 - a_1)\tau_2$. In the cases of the densities of 1.4 and 1.6 ρ_c data from duplicate runs performed on different days are shown as an indication of the precision of the results.

TABLE 2: Properties of Solutes Used in the Simulation and Calculated Parameters[a]

solute	V_{vdW}/Å^3	μ/D	$\langle N_1\rangle$	$\langle U_{LJ}\rangle$/kJ mol^{-1}	$\langle U_{El}\rangle$/kJ mol^{-1}	$\langle\Delta E_{el}\rangle/10^3$ cm^{-1}
C153 S_0	246	6.24	48.5	−94.08	−20.99	−0.691
C153 S_1	246	13.59	49.3	−99.38	−59.06	−2.483
DCS S_0	217	8.35	52.8	−96.95	−31.60	−0.262
DCS S_1	217	15.74	54.0	−105.85	−49.87	−1.161

[a] V_{vdW} is the van der Waals volume and μ the dipole moment of the model solutes. The remaining quantities are average values simulated at the highest solvent density $2.0\rho_c$. N_1 is the coordination number, U_{El} the electrostatic and U_{LJ} the Lennard-Jones component of the solute−solvent interaction energy, and ΔE_{el} the electrical energy gap (eq 3.)

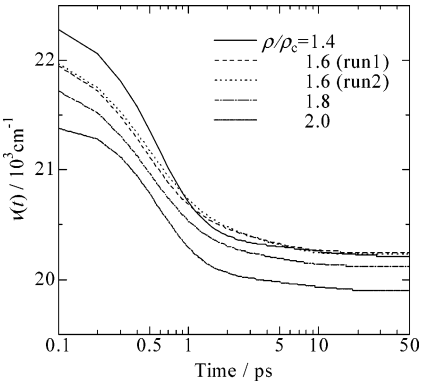

Figure 4. Time-dependent frequency shift of DCS in supercritical CHF_3 at 310 K at several densities.

in which $\nu(0)$, $\nu(\infty)$, τ_1, and τ_2 are fitting parameters. Table 1 also shows the integral time constants $\langle\tau\rangle = a_1\tau_1 + (1 - a_2)\tau_2$ and the value of $\nu(0)_{est}$ estimated from the steady-state spectra. We note that the values of $\nu(\infty)$ listed here are all approximately 200 cm^{-1} smaller than the steady-state values plotted in Figure 2. This difference results from imperfections in the spectral correction of the Kerr data of the sort described in ref 41 and not to a lack of equilibration in the steady-state emission. With the exception of the highest density point, the apparent values of $\nu(0)$ also differ from the steady-state estimates $\nu(0)_{est}$ by approximately this same amount. This observation, together with the ±300 cm^{-1} uncertainty in $\nu(0)_{est}$, the data in Table 1, suggests that we capture most (>90%) if not all of the solvation dynamics occurring in these systems. It is interesting that the observed dynamics are not very sensitive to density over the range from $1.4\rho_c$ to $2.0\rho_c$. Both τ_1 and $\langle\tau\rangle$ are almost density-independent. It appears that τ_2 may have a minimum at $\rho/\rho_c = 1.6$, but the observed variations are not much larger than the anticipated uncertainties in the data.

5. Simulation Results and Comparison to Experiment

We begin by comparing the simulated spectral shifts to experimental data. Because the steady-state data obtained with the probe C153 are of higher quality than those obtained with DCS, as well as for comparison's sake, we have simulated the spectra and dynamics of both DCS and C153. Parts A and B of Figure 5 show C153 results. The solvent-induced shifts in the

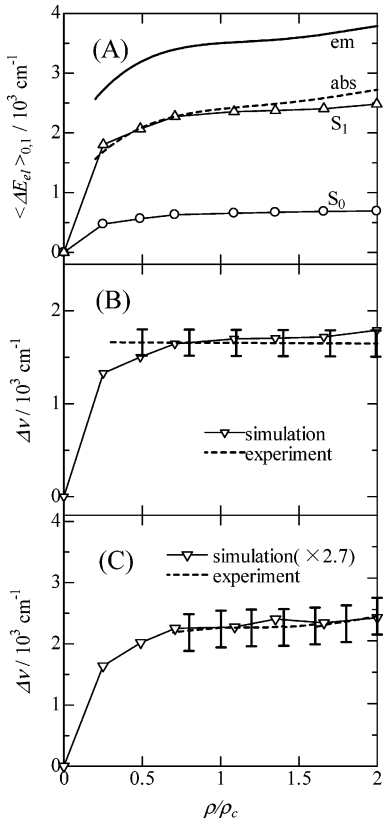

Figure 5. Comparison of experimental (dashed curves) and simulated (connected points) spectral shifts of C153 and DCS in CHF_3 at 310 K as functions of density. (A) C153 absorption and emission shifts relative to the gas phase, (B) C153 Stokes shifts, and (C) DCS Stokes shifts. In panel C, the simulated data (connected points) have been scaled by a factor of 2.7 (see text). Experimental C153 data are from ref 59.

absorption and emission frequencies, $\Delta\nu_{abs}$ and $\Delta\nu_{em}$, calculated using eqs 4 and 5 are plotted as functions of density in Figure 5A. The experimental results previously reported by Biswas et al.[59] are also plotted as solid and dashed lines. The simulations clearly underestimate the solvent-induced shifts, particularly $\Delta\nu_{abs}$. This poor agreement is to be expected because the absorption and emission shifts are sensitive to solvent electronic polarizability[61,62] as well as to the interactions due to the permanent charge distributions of solvent molecules modeled

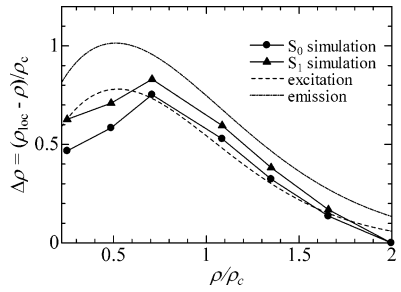

Figure 6. Experimental (smooth dashed curves) and simulated (connected points) magnitudes of the local density augmentation of C153 in supercritical CHF_3 in the ground and excited states.

here. The density dependence of the shifts is nevertheless reasonably reproduced for both $\Delta\nu_{abs}$ and $\Delta\nu_{em}$. Figure 5B compares the experimental (dashed line and error bars) and simulated Stokes shifts (connected points) of C153, calculated using eq 6. As in the case of DCS, the experimental Stokes shift of C153 is nearly independent of density over a relatively wide range of densities, between $0.3\rho_c$ and $2.0\rho_c$.[59] The simulations show a slightly larger density dependence than the experiments, but the dependence is still modest (~25%) over the experimental data range. In contrast to the individual absorption and emission shifts, the magnitude of the Stokes shift is accurately reproduced by the simulations. We take this agreement as an indication that the Stokes shift and its density dependence are largely accounted for by the electrical interactions ΔE_{el} modeled in terms of eq 3.

The experimental and simulated Stokes shifts of DCS are compared in Figure 5C. (The simulated frequency shifts of DCS are similar to those displayed in Figure 5A, but we do not display them because the gas-phase references needed to compare the experimental data are not available.) As seen for C153, the simulated Stokes shift of DCS is only weakly dependent on density down to $0.5\rho_c$, after which it decreases quickly to zero. However, in the DCS case the simulated magnitudes of the Stokes shifts are far less than the experimentally measured values. As illustrated in Figure 3C, good agreement between simulation and experiment requires that the simulated Stokes shifts be scaled up by a factor of 2.7. We do not believe that this quantitative discrepancy between simulation and experiment indicates a failure of eq 3 but instead indicates that the charge distribution we employ for DCS is not sufficiently accurate. The dipole moments of the DCS charge distributions used in the present simulations are 8.3 and 15.7 D in S_0 and S_1, respectively (Table 2), so that $\Delta\mu_{sim} = 7.4$ D. Electrochromic and solvatochromic measurements[42,45,54] indicate a much larger difference of ~13 D between S_0 and S_1. The underestimation of $\Delta\mu$ in the simulation model would be expected to cause the simulated Stokes shifts to be too small by roughly a factor of $(\Delta\mu_{exp}/\Delta\mu_{sim})^2 = 3$, which agrees with the present observation.

We next examine the local density augmentation around C153 in CHF_3. The results obtained from these simulations and prior experiments[59] are displayed in Figure 6. Density augmentation is estimated from the simulations using solvation shell distribution functions, $g_{ss}(r)$, as described by Patel and Maroncelli.[14] $g_{ss}(r)$ represents the relative probability of finding a solvent atom at a distance r away from the nearest solute atom, independent of the identity of the solute or solvent atoms. The first shell coordination number N_1 is calculated by integrating $g_{ss}(r)$ out to the position of the first minimum observed at the highest density. Local densities ρ_{loc} are then determined from N_1 by assuming equality of the local and bulk densities at a reference density $\rho_{ref} = 2\rho_c$ using the relation

$$\rho_{loc}(\rho) \equiv \frac{N_1(\rho)}{N_1(\rho_{ref})}\rho_{ref} \tag{10}$$

In Figure 6, we show values of the density augmentation defined by $\Delta\rho = (\rho_{loc} - \rho)/\rho_c$ to emphasize the departure from bulk conditions. As illustrated in Figure 6 there is reasonably good agreement between the simulated values of $\Delta\rho$ and the effective local solvent densities around C153 in S_0 and S_1 deduced from the density dependence of the excitation and emission frequencies.[59] The magnitude and location of the maximum in $\Delta\rho$ as well as the slightly greater augmentation in S_1 are similar in experiment and simulation. The density augmentation of DCS obtained from simulation is comparable to that shown in Figure 6 for C153, $\Delta\rho_{max}$ is predicted to be 0.78 in S_0 and 0.88 in S_1, but the data are not plotted because of the absence of adequate experimental data.

The comparisons in Figures 5 and 6 suggest that the simulations of C153, and by analogy DCS, provide reasonable representations of the structure ($\Delta\rho$) and spectroscopy of these two solutes. We therefore now turn to a description of the simulated dynamics. We first survey the density dependence of several different time-correlation functions potentially relevant to the solvation dynamics. All are normalized functions of the sort

$$C_A(t) = \frac{\langle \delta A(0)\delta A(t)\rangle}{\langle \delta A^2\rangle} = C[A] \tag{11}$$

where $\delta A(t) = A(t) - \langle A\rangle$ is the fluctuation in some property A at time t. The four observables whose dynamics we examine are the coordination number N_1 described above, the electrostatic contribution to the energy gap ΔE_{el} defined by eq 3, the Lennard-Jones portion of the solute−solvent interaction energy U_{LJ}, and the dispersion component of U_{LJ}, defined by

$$U_{disp} = -4\sum_{i,\alpha}\epsilon_{i\alpha}\left(\frac{\sigma_{i\alpha}}{r_{i\alpha}}\right)^6 \tag{12}$$

where i and α label solvent and solute sites and ϵ and σ are the site−site Lennard-Jones parameters. As indicated in eq 11, we will refer to the various correlation functions as $C[N_1]$, $C[\Delta E_{el}]$, etc.

Figure 7 shows the results obtained with DCS in the S_1 state at four densities. Table 3 summarizes some of the characteristics of these time correlation functions. Comparing the various functions, one notes a remarkable difference between the dynamics of electrical interactions ΔE_{el} used to model the solvation dynamics, and the dynamics of the remaining observables. The $C[\Delta E_{el}]$ functions all decay to near zero within about 200 fs via a pronounced Gaussian component and then show damped oscillations about zero. These features are observed at all densities, and there is little difference among the $C[\Delta E_{el}]$ except at the lowest density studied, $0.25\rho_c$. In contrast, the correlation functions of N_1, U_{LJ}, and U_{disp} do not show such a pronounced Gaussian component or the oscillations found in $C[\Delta E_{el}]$. The latter functions are reasonably represented as biexponential functions of time and all exhibit long-time components which vary systematically with solvent density (Table 3). We have not attempted to dissect these correlation functions into translational and rotational contributions,[63] but it seems reasonable to attribute the marked difference between $C[\Delta E_{el}]$ and the other correlation functions to the differential

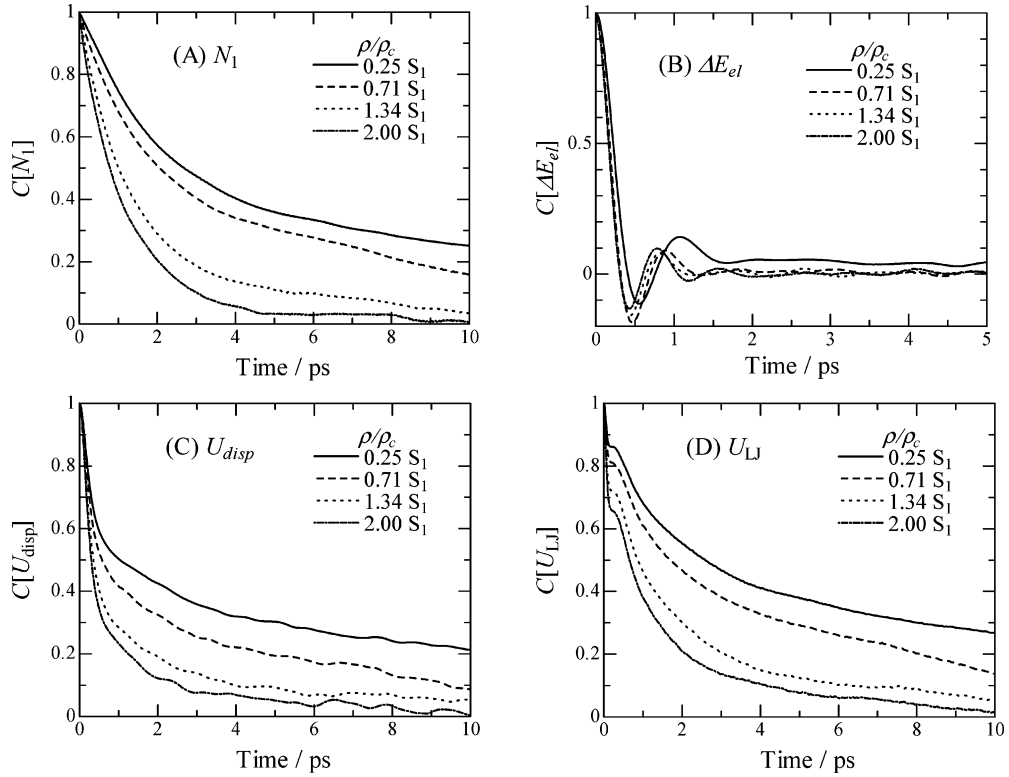

Figure 7. Time correlation functions of (A) N_1, (B) ΔE_{el}, (C) U_{disp}, and (D) U_{LJ} of DCS in the excited state.

TABLE 3: Characteristic Parameters of the Time Correlation Functions Simulated for S_1 DCS[a]

	$C[\Delta E_{el}]$	$C[N_1]$			$C[U_{LJ}]$			$C[U_{disp}]$		
ρ/ρ_c	τ_{1e}/ps	a_1	τ_1/ps	τ_2/ps	a_1	τ_1/ps	τ_2/ps	a_1	τ_1/ps	τ_2/ps
0.25	0.26	0.618	2.01	23.71	0.464	1.13	13.96	0.550	0.49	13.63
0.49	0.23	0.525	1.63	9.95	0.433	0.89	8.09	0.559	0.39	7.34
0.71	0.21	0.494	1.26	9.17	0.447	0.78	7.83	0.634	0.47	8.39
1.09	0.21	0.553	1.16	6.42	0.425	0.63	5.14	0.640	0.38	5.67
1.35	0.20	0.774	1.09	6.34	0.676	0.82	5.56	0.714	0.36	4.44
1.66	0.20	0.880	1.16	8.12	0.429	0.57	2.50	0.609	0.30	2.28
2.00	0.19	0.908	1.04	5.05	0.689	0.62	3.72	0.749	0.33	3.00

[a] τ_{1e} denotes the time at which $C(t)$ reaches a value of e^{-1} and a_1, τ_1, and τ_2 denote parameters of biexponential fits of the correlation functions to the form $C(t) = a_1 \exp(-t/\tau_1) + (1 - a_1) \exp(- t/\tau_2)$. For $C[U_{LJ}]$, we fit only the data at times longer than 0.3 ps.

role played by these two types of solvent motions. We anticipate that the electrical correlation functions are dominated by the fast rotational dynamics of solvent molecules, which are apparently sufficient for almost complete relaxation. The interactions which relax fluctuations of the coordination number N_1 and the nonpolar energies U_{LJ} and U_{disp} are of a different symmetry from the electrical interactions[64] and are much less sensitive to rotational motion. Apparently, the greater contribution of translational solvent motions leads to much slower, density dependent long-time tails in these latter correlation functions.

Quite similar correlation functions to those displayed in Figure 7 are simulated for DCS in S_0 as well as for C153 in S_0 and S_1. (These results are provided in the Supporting Information.) No significant differences are observed between the correlation functions simulated for the S_0 and S_1 states of these solutes except that $C[\Delta E_{el}]$ in S_1 at the lowest density displays a small tail at long times (Figure 7B), which is not observed in the S_0 functions. Such similarity between the S_1 and S_0 correlation functions, as well as the fact that the magnitudes of the shifts calculated using eq 6 are within 10−15% of the observed values, suggest that the linear response assumption is appropriate for these systems. (It should, however, be remembered that the present DCS simulations significantly underestimate the differences between the S_0 and S_1 charge distributions and for this reason would be expected to also underestimate any nonlinear behavior.) It is also notable that the dynamics probed by C153 and DCS are very similar, indicating that details of the solute molecular structure and charge distribution have little impact on the basic features of the simulated dynamics.

We finally turn to a comparison of the experimental and simulated dynamics, which is made in Figure 8. Figure 8A compares $S_\nu(t)$ to $C[\Delta E_{el}]$. If the spectral dynamics reflect only electrical interactions as described in section 3, and if the linear response approximation is valid, these two functions should be directly comparable. As shown in Figure 8A, the correspondence between the two functions is poor. The prominent Gaussian decay of $C[\Delta E_{el}]$ leads to a $1/e$ time of 230 fs, whereas the corresponding time of $S_\nu(t)$ is roughly twice this value, 450 fs. More importantly, the pronounced oscillations in $C[\Delta E_{el}]$ are not observed in the experimental response and the ∼10% long-time tail observed in experiment is completely absent in the simulated correlation function.

There are a number of possible origins of this disagreement between simulation and experiment. The KGE experiment used here has an instrumental response of 450 fs fwhm, which could potentially mask some of the fastest dynamics present. We do not believe that this is a primary source of the difference for

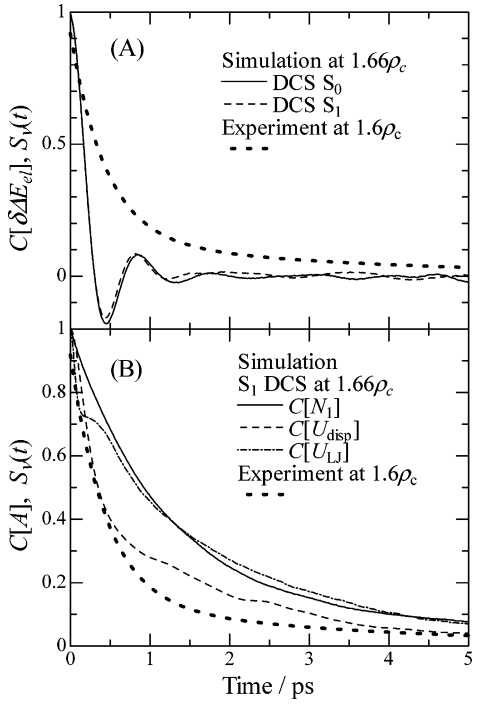

Figure 8. Comparisons of the experimental spectral response function $S_\nu(t)$ (averaged over two runs at 1.6ρ_c) and various simulated time correlation functions (1.66ρ_c).

two reasons. First, the data used for constructing the experimental $S_\nu(t)$ response have been fit to remove instrumental broadening and previous tests have shown that such fitting methods are capable of reliably recovering spectral dynamics as fast as 100 fs.[41] Furthermore, the magnitudes of the Stokes shifts we observe are within 10% of the solvation Stokes shifts estimated from independent spectral data. It is therefore unlikely that we have missed any substantial ultrafast component of the sort appearing in $C[\Delta E_{el}]$.

One can always point to inaccuracies in the potential functions used in simulation as a possible source of such discrepancies. Recent simulations by Ingrosso and Ladanyi[34] suggest that this possibility is indeed part of the answer in the present case. Ingrosso and Ladanyi performed molecular dynamics simulations of C153 in supercritical CHF_3 using both the two-site model of fluoroform employed here as well as an all-atom (five-site) model. The electrical correlation functions $C[\Delta E_{el}]$ they calculate using the two solvent models are markedly different. Most notably, the all-atom model does not exhibit the oscillations in $C[\Delta E_{el}]$ found with the two-site model, and unlike the two-site model, the correlation functions predicted by the all-atom model possess a ~10% long-time tail similar to what is observed in experiment.[34] Thus, an all atom representation yields $C[\Delta E_{el}]$ functions that are qualitatively much closer to the experimental $S_\nu(t)$ than does the reduced representation of fluoroform employed here. However, the dynamics of ΔE_{el} simulated with the five-site model still show some quantitative differences compared to the experimental results. As in the two-site model described here, there is a pronounced Gaussian component of the simulated dynamics which leads to a $1/e$ time much faster (again ~200 fs) than what is observed in experiment (~450 fs).

We speculate that this remaining difference is the result of lack of explicit solvent polarizability in the simulation model. Such polarizability would have two effects. First, polarizability tends to soften the solvation "force constant" and lead to slower dynamics than found in comparable nonpolarizable systems.[65,66] In addition, inductive interactions between the solute and solvent would increase the importance of "symmetric" interactions (ones which do not distinguish between the + and − ends of the diatomic solvent molecules). Figure 8B and Table 3 show that all of the other correlation functions considered, which are of a symmetric variety and presumably involve more translational contributions, show slower initial decays and more substantial long time tails and thus bear more resemblance to $S_\nu(t)$ than does $C[\Delta E_{el}]$. We note that the time constants of the slower parts of the dynamics observed in experiment are quite close to those of the nonelectrical correlation functions, especially $C[U_{disp}]$. Thus, it seems likely that addition of solvent polarizability would increase the contribution of translational motions in the response and lead to a simulated spectral dynamics intermediate between the dynamics of $C[\Delta E_{el}]$ and the other correlation functions examined here. As illustrated in Figure 8, such intermediate behavior is what is observed of the experimental response. Simulations with polarizable solvent and solute models are needed to decide whether this speculation is correct or not.

Finally, before closing, it is of interest to compare the present results with the prior measurements of Kimura[38] and others,[39] who reported much slower, ~50 ps components in the solvation of C153 in supercritical CHF_3. We do not find times longer than about 10 ps in the DCS experiments or in the simulations of either DCS or C153. It is possible that we have missed some small-amplitude dynamics at times greater than 10 ps in the experiments as a result of the short lifetime of DCS (~100 ps) and signal-to-noise limitations at longer times. However, we note that the previous experiments only observed these slower times at densities lower than those accessible here, and it seems more likely that we have observed essentially all of the dynamics that are present in the density range studied. It is not clear why the simulated dynamics at the lower densities do not indicate the presence of such slow dynamics.

6. Conclusions

We have used femtosecond KGE spectroscopy with the solute DCS to provide the first complete measurements of the fast solvation dynamics present in supercritical CHF_3 near the critical point ($T = 310$ K; 1.04 T_c). These experiments appear to have captured most (> 90%) if not all of the dynamics occurring over the accessible density range between 1.4ρ_c and 2.0ρ_c. The measured spectral response $S_\nu(t)$ exhibits a bimodal decay with ~0.6 and ~9 ps components and only a modest density dependence between 1.4ρ_c and 2.0ρ_c. Molecular dynamics simulations have also been performed on systems consisting of both C153 and DCS in a diatomic model of supercritical CHF_3. Although the simulations provide a reasonable account of the magnitude of the solvation response, the dynamics simulated based on permanent electrical interactions alone are faster than those observed experimentally. Part of the discrepancy results from oversimplification of the shapes of solvent molecules in the 2-site model employed here. We conjecture that neglect of solvent polarizability and thereby inductive components of the solvation energy may also play a role in the lack of agreement found even with all-atom solvent models.[34]

Acknowledgment. The authors thank Klaas Zachariasse for providing the sample of DCS used here and Francesca Ingrosso and Branka Ladanyi for sharing the results of their simulations prior to publication as well as for many fruitful discussions. This work was funded by a grant from the US National Science Foundation (to M.M.).

Supporting Information Available: Tables giving all potential parameters used in the simulation and figures showing correlation functions simulated for DCS in S_0 and for C153 in S_0 and S_1. This material is available free of charge via the Internet at http://pubs.acs.org.

References and Notes

(1) Noyori, R., Ed. *Chem. Rev.* **1999**, *99*, 353.
(2) Tucker, S. C. *Chem. Rev.* **1999**, *99*, 391.
(3) Kajimoto, O. *Chem. Rev.* **1999**, *99*, 355.
(4) Song, W.; Biswas, R.; Maroncelli, M. *J. Phys. Chem. A* **2000**, *104*, 6924.
(5) Kimura, Y.; Yamamoto, Y.; Terazima, M. *J. Chem. Phys.* **2005**, *123*, 054512.
(6) Egorov, S.; Lawrence, C. P.; Skinner, J. L. *J. Phys. Chem. B* **2005**, *109*, 6879.
(7) Roychowdhury, S.; Bagchi, B. *J. Chem. Phys.* **2003**, *119*, 3278.
(8) Sekiguchi, K.; Shimojima, A.; Kajimoto, O. *Chem. Phys. Lett.* **2002**, *356*, 84.
(9) Myers, D. J.; Shigeiwa, M.; Cherayil, B. J.; Fayer, M. D. *J. Chem. Phys.* **2001**, *115*, 4689.
(10) Vikhrenko, V. S.; Schwarzer, D.; Schroeder, J. *Phys. Chem. Chem. Phys.* **2001**, *3*, 1000.
(11) Egorov, S. A. *J. Chem. Phys.* **2003**, *119*, 4798.
(12) Ohmori, T.; Kimura, Y.; Hirota, N.; Terazima, M. *J. Phys. Chem. B* **2003**, *107*, 5958.
(13) Ohmori, T.; Kimura, Y. *J. Chem. Phys.* **2003**, *119*, 7328.
(14) Patel, N.; Biswas, R.; Maroncelli, M. *J. Phys. Chem. B* **2002**, *106*, 7096.
(15) Brennecke, J. F.; Chateauneuf, J. E. *Chem. Rev.* **1999**, *99*, 433.
(16) Ladanyi, B. M.; Nugent, S. *J. Chem. Phys.* **2006.**
(17) Kapko, V.; Egorov, S. A. *J. Chem. Phys.* **2004**, *121*, 11145.
(18) Egorov, S. A. *Phys. Rev. Lett.* **2004**, *93*, 23004.
(19) Egorov, S. A. *J. Chem. Phys.* **2004**, *121*, 6948.
(20) Egorov, S. A. *J. Chem. Phys.* **2003**, *118*, 10643.
(21) Egorov, S. A.; Stephens, M. D.; Skinner, J. L. *J. Chem. Phys.* **1997**, *107*, 10485.
(22) Stephens, M. D.; Saven, J. G.; Skinner, J. L. *J. Chem. Phys.* **1997**, *106*, 2129.
(23) Larregaray, P.; Cavina, A.; Chergui, M. *Chem. Phys.* **2005**, *308*, 13.
(24) Marques Martins, M.; Stassen, H. *J. Chem. Phys.* **2003**, *118*, 5558.
(25) Yamaguchi, T.; Kimura, Y.; Nakahara, M. *J. Phys. Chem. B* **2002**, *106*, 9126.
(26) Yamaguchi, T.; Kimura, Y.; Hirota, N. *J. Chem. Phys.* **1999**, *111*, 4169.
(27) Maddox, M.; Goodyear, G.; Tucker, S. *J. Phys. Chem. B* **2000**, *104*, 6266.
(28) Noworyta, J. P.; Koneshan, S.; Rasaiah, J. C. *J. Am. Chem. Soc.* **2000**, *122*, 11194.
(29) Graf, P.; Nitzan, A. *Chem. Phys.* **1998**, *235*, 297.
(30) Re, M.; Laria, D. *J. Phys. Chem. B* **1997**, *101*, 10494.
(31) Kalbfleisch, T. S.; Ziegler, L. D.; Keyes, T. *J. Chem. Phys.* **1996**, *105*, 7034.
(32) Kalbfleisch, T.; Fan, R.; Roebber, J.; Moore, P.; Jacobsen, E.; Ziegler, L. D. *J. Chem. Phys.* **1995**, *103*, 7673.
(33) Heidelbach, C.; Vikhrenko, V. S.; Schwarzer, D.; Schroeder, J. *J. Chem. Phys.* **1999**, *110*, 5286.
(34) Ingrosso, F.; Ladanyi, B. M. Solvation Dynamics of C153 in Supercritical Fluoroform: A Simulation Study Based on 2-Site and 5-Site Models of the Solvent. To be submitted for publication.
(35) Ingrosso, F.; Ladanyi, B. M.; Mennucci, B.; Scalmani, G. Solvation of C153 in Supercritical Fluoroform. *J. Chem. Phys.*, in press.
(36) Betts, T. A.; Zagrobelny, J.; Bright, F. V. *J. Supercrit. Fluids* **1992**, *5*, 48.
(37) Bhattacharyya, K.; Hara, K.; Kometani, N.; Uozu, Y.; Kajimoto, O. *Chem. Phys. Lett.* **2002**, *361*, 136.
(38) Kimura, Y.; Hirota, N. *J. Chem. Phys.* **1999**, *111*, 5474.
(39) Ronne, C.; Biswas, R.; Maroncelli, M. Unpublished results 1999.
(40) Kimura, Y.; Saga, N. *J. Mol. Liq.* **2005**, *119*, 113.
(41) Arzhantsev, S.; Maroncelli, M. *Appl. Spectrosc.* **2005**, *59*, 206.
(42) Il'ichev, Y. V.; Kühnle, W.; Zachariasse, K. A. *Chem. Phys.* **1996**, *211*, 441.
(43) Il'ichev, Y. V.; Zachariasse, K. A. *Ber. Bunsen-Ges. Phys. Chem.* **1997**, *101*, 625.
(44) Kovalenko, S. A.; Schanz, R.; Senyushkina, T. A.; Ernsting, N. P.*Phys. Chem. Chem. Phys.* **2002**, *4*, 703.
(45) Arzhantsev, S.; Zachariasse, K.; Maroncelli, M. The Photophysics of Dimethylaminocyanostilbene and its use as a Solvation Probe. Submitted to *J. Phys. Chem. B.*, in press.
(46) Song, W.; Patel, N.; Maroncelli, M. *J. Phys. Chem. B* **2002**, *106*, 8783.
(47) Shimojima, A.; Amita, F.; Kajimoto, O. To be submitted to *Rev. Sci. Instrum.*
(48) DL_POLY_2, Smith, W.; Forester, T. R., Eds.; CCLRC Daresbury Laboratory: Daresbury, U.K., 2001.
(49) Frenkel, D.; Smit, B. *Understanding Molecular Simulation, From Algorithms to Applications*, 2nd ed.; Academic Press: New York, 2002.
(50) Gaussian 03, Revision C.01. Frisch, M. J.; Trucks, G. W.; Schlegel, H. B.; Scuseria, G. E.; Robb, M. A.; Cheeseman, J. R.; Montgomery, J. A., Jr.; Vreven, T.; Kudin, K. N.; Burant, J. C.; Millam, J. M.; Iyengar, S. S.; Tomasi, J.; Barone, V.; Mennucci, B.; Cossi, M.; Scalmani, G.; Rega, N.; Petersson, G. A.; Nakatsuji, H.; Hada, M.; Ehara, M.; Toyota, K.; Fukuda, R.; Hasegawa, J.; Ishida, M.; Nakajima, T.; Honda, Y.; Kitao, O.; Nakai, H.; Klene, M.; Li, X.; Knox, J. E.; Hratchian, H. P.; Cross, J. B.; Adamo, C.; Jaramillo, J.; Gomperts, R.; Stratmann, R. E.; Yazyev, O.; Austin, A. J.; Cammi, R.; Pomelli, C.; Ochterski, J. W.; Ayala, P. Y.; Morokuma, K.; Voth, G. A.; Salvador, P.; Dannenberg, J. J.; Zakrzewski, V. G.; Dapprich, S.; Daniels, A. D.; Strain, M. C.; Farkas, O.; Malick, D. K.; Rabuck, A. D.; Raghavachari, K.; Foresman, J. B.; Ortiz, J. V.; Cui, Q.; Baboul, A. G.; Clifford, S.; Cioslowski, J.; Stefanov, B. B.; Liu, G.; Liashenko, A.; Piskorz, P.; Komaromi, I.; Martin, R. L.; Fox, D. J.; Keith, T.; Al-Laham, M. A.; Peng, C. Y.; Nanayakkara, A.; Challacombe, M.; Gill, P. M. W.; Johnson, B.; Chen, W.; Wong, M. W.; Gonzalez, C.; Pople, J. A. Gaussian, Inc.: Wallingford CT, 2004.
(51) Muhlpfordt, A.; Schanz, R.; Ernsting, N.; Farztdinov, V.; Grimme, S. *Phys. Chem. Chem. Phys.* **1999**, *1*, 3209.
(52) AMPAC8, 6.55 ed. Semichem Inc.: Shawnee KS, 2004.
(53) Jorgensen, W. L.; Maxwell, D. S.; Tirado-Rives, J. *J. Am. Chem. Soc.* **1996**, *118*, 11225.
(54) Liptay, W. Dipole Moments and Polarizabilities of Molecules in Excited Electronic States In *Excited States*; Lim, E. C., Ed.; Academic Press: New York, 1974; Vol. 1, pp 129−229.
(55) Kanya, R.; Ohshima, Y. *Chem. Phys. Lett.* **2003**, *370*, 211.
(56) Chowdhury, A.; Locknar, S. A.; Premvardhan, L. L.; Peteanu, L. A. *J. Phys. Chem. A* **1999**, *103*, 9614.
(57) Fee, R. S.; Maroncelli, M. *Chem. Phys.* **1994**, *183*, 235.
(58) Betts, T. A.; Zagrobelny, J.; Bright, F. V. *J. Am. Chem. Soc.* **1992**, *114*, 8163.
(59) Biswas, R.; Lewis, J.; Maroncelli, M. *Chem. Phys. Lett.* **1999**, *310*, 485.
(60) Lewis, J.; Biswas, R.; Robinson, A.; Maroncelli, M. *J. Phys. Chem. B* **2001**, *105*, 3306.
(61) Horng, M. L.; Gardecki, J. A.; Papazyan, A.; Maroncelli, M.; *J. Phys. Chem.* **1995**, *99*, 17311.
(62) Reynolds, L.; Gardecki, J. A.; Frankland, S. J. V.; Horng, M. L.; Maroncelli, M. *J. Phys. Chem.* **1996**, *100*, 10337.
(63) Ladanyi, B. M.; Maroncelli, M. *J. Chem. Phys.* **1998**, *109*, 3204.
(64) Ladanyi, B. M.; Stratt, R. M. *J. Phys. Chem.* **1996**, *100*, 1266.
(65) Bursulaya, B.; Zichi, D. A.; Kim, H. J. *J. Phys. Chem.* **1995**, *99*, 10069.
(66) Kumar, P. V.; Maroncelli, M. *J. Chem. Phys.* **1995**, *103*, 3038.